ACADEMIC PRESS

Available online at www.sciencedirect.com
SCIENCE DIRECT®

Journal of Catalysis 214 (2003) 15–25

JOURNAL OF CATALYSIS

www.elsevier.com/locate/jcat

Liquid phase hydrogenation of acetonitrile to ethylamine over the Co–B amorphous alloy catalyst

Hexing Li,* Yuedong Wu, Hongshan Luo, Minghui Wang, and Yeping Xu

Department of Chemistry, Shanghai Normal University, Shanghai 200234, People's Republic of China

Received 1 May 2002; revised 3 October 2002; accepted 7 October 2002

Abstract

The Co–B amorphous alloy catalyst was prepared by chemical reduction of Co^{2+} ions with BH_4^- in aqueous solution. Its activity and selectivity were measured during the liquid phase hydrogenation of acetonitrile and the effects of various factors, such as the reaction time, acetonitrile concentration, hydrogen pressure, reaction temperature, and solvent, were investigated. The following results were obtained: (1) The maximum ethylamine yield of 69% was obtained at the total conversion of acetonitrile. (2) The acetonitrile hydrogenation was zero-order with respect to acetonitrile and first-order with respect to hydrogen. Meanwhile, the selectivity to ethylamine increased slightly with the increase of either hydrogen pressure or acetonitrile concentration. (3) Increased reaction temperature resulted in a great enhancement in the activity (the apparent activation energy was determined as 46 kJ/mol) but a slight decrease in the selectivity to ethylamine. (4) Addition of a little H_2O may result in an increase in the activity. All these effects are discussed based on the reaction mechanism. In comparison with other Co-based catalysts, such as Raney Co, pure Co powder catalyst, and the crystallized Co–B catalyst, the amorphous Co–B catalyst exhibited much higher activity and better selectivity to ethylamine. Although Ni-based catalysts had higher activity, their poorer selectivity to ethylamine suggested that they were not suitable for the title reaction under the present conditions. Based on the reaction mechanism and various characterizations, including SAED, XRD, SEM, TEM, EXAFS, XPS, hydrogen chemisorption, and DSC, the promoting effects on the activity and selectivity of the Co–B amorphous catalyst are discussed briefly by considering both the structural characteristics and the electronic interaction between the Co and the alloying B.

Keywords: Acetonitrile; Hydrogenation; Condensation; Ethylamine; Co–B amorphous catalyst

1. Introduction

Hydrogenation of nitriles is widely used in industry to produce diverse amines, as in the hydrogenation of adiponitrile, stearonitrile, lauronitrile, and benzonitrile to the corresponding hexamethylenediamine, stearylamine, dodecylamine, and benzylamine. Ni- and Co-based catalysts are most frequently employed for the production of primary amines [1–5]. However, the hydrogenation of acetonitrile (CH_3CN) to ethylamine is seldom employed in traditional industry due to the high cost and nonavailability of CH_3CN at early time. The ethylamine is mainly produced via the following reaction:

$$CH_3CH_2OH + NH_3 \rightarrow CH_3CH_2NH_2 + H_2O.$$

Recently, the hydrogenation of CH_3CN has caused much attention owing to the rapid development of the acrylonitrile industry, which results in the accumulation of more and more CH_3CN, since it is a main byproduct during acrylonitrile production (10% w/w). As is well known, nitrile hydrogenation usually results in a mixture of compounds consisting mostly of primary, secondary, and tertiary amines [6]. Although both ethylamine (primary amine) and diethylamine (secondary amine), as well as triethylamine (tertiary amine), are important owing to their unique applications, selectivity is still of chief interest in acetonitrile hydrogenation in order to obtain a high yield of the desired product and to avoid the difficult separation procedure. Here, we choose the selective hydrogenation of acetonitrile to ethylamine since, on one hand, it is relatively simpler; on the other hand, both the secondary and tertiary amines could easily be prepared from the primary amine [6]. Regarding various affecting factors, the catalyst plays a decisive role in determining the selectivity to the desired products [2]. How-

* Corresponding author.
E-mail address: HeXing-Li@shtu.edu.cn (H. Li).

0021-9517/03/$ – see front matter
doi:10.1016/S0021-9517(02)00038-6

ever, only a few catalysts suitable for CH_3CN hydrogenation to the primary amine (ethylamine, $C_2H_5NH_2$) have been reported so far [7–11]. Since the 1980s, amorphous alloys have been widely used in hydrogenation reactions owing to their higher activity, better selectivity, and stronger sulfur resistance in comparison with the corresponding crystalline metal catalysts [12–15]. Most studies focus on the Ni-based amorphous catalysts. The hydrogenation of adiponitrile over Ni–B and Ni–P amorphous alloy catalysts has been reported previously [16–18]. But these Ni-based amorphous catalysts are not suitable for acetonitrile hydrogenation due to their poor selectivity to primary amine. We report here an ultrafine Co–B amorphous alloy which seems to have potential for the hydrogenation of CH_3CN to $C_2H_5NH_2$ in liquid phase.

2. Experimental

2.1. Catalyst preparation

The Co–B sample with the composition $Co_{75.4}B_{24.6}$ (atomic ratio) was prepared by chemical reduction according to the method described in our previous papers [19,20]. Briefly, 48 ml of 2.0 M KBH_4 solution containing 0.20 M NaOH was added dropwise into 30 ml of aqueous solution of $CoCl_2$ containing 1.5 g Co under vigorous stirring. As the reduction is strongly exothermic, the KBH_4 solution was added very slowly (1.5 ml/min) and the reaction was performed at 273 K in an ice-water bath to prevent local overheating, which may cause the gathering of small particles and/or the crystallization of the Co–B amorphous alloy. The KBH_4 was greatly excessive (the molar ratio between the cobalt and KBH_4 was about 4:1) and the reaction mixture was stirred for enough time to ensure the complete reduction of the Co^{2+} in the solution. The resulting black solid was washed free from Cl^- and K^+ ions with distilled H_2O (until pH 7 was obtained), during which some soluble boron species were also removed. Then it was washed further with absolute alcohol (EtOH), and finally it was stored in EtOH until use. The pure Co powders were prepared by using NH_2NH_2 instead of KBH_4 for the reaction of Co^{2+} at 363 K. Heating pretreatment of the Co–B sample was carried out in N_2 flow at different temperatures for 2.0 h, respectively. The Ni–B amorphous alloy was prepared in a way similar to that described for the Co–B preparation. It was found that the B content in the Ni–B sample increased with increased of the KBH_4 concentration. Thus, the $Ni_{80.7}B_{19.3}$, $Ni_{75.2}B_{24.8}$, and $Ni_{66.7}B_{33.3}$ samples were prepared using aqueous solutions containing 0.5, 1.0, and 2.0 M KBH_4, respectively. However, the Co–B sample with B content higher than 24.6% or the Ni–B sample with B content higher than 33.3% could not be obtained through chemical reduction under the present conditions due to the limitation of the solubility of KBH_4 in H_2O. For comparison, Raney Co and Raney Ni catalysts were also prepared by alkali leaching the commercially available Co–Al and Ni–Al alloys (50/50, w/w), respectively.

2.2. Catalyst characterization

The amorphous structure of the Co–B catalysts was determined by X-ray powder diffraction (XRD, Bruker AXS D8-Advance with Cu-K_α radiation), selective area electronic diffraction (SAED, JEM-2010), and extended X-ray absorption fine structure (EXAFS, BL-10B) carried out in the National Laboratory of High Energy Physics (KEK, Tsukuba, Japan). The crystallization of the Co–B sample was followed by differential scanning calorimetry (DSC, Perkin–Elmer) under N_2 atmosphere at a heating rate of 10 K/min. The surface morphology and particle sizes of amorphous Co–B alloy were observed by a scanning electron micrograph (SEM, XL 30 Philips) and a transmission electron micrograph (TEM, JEM-2010). The composition of the Co–B sample was analyzed by means of inductively coupled plasma (ICP, Jarrell-As Scan 2000). The active surface area (S_{act}) was determined by H_2 chemisorption, as described previously [21]. X-ray photoelectron spectroscopy (XPS) was performed on a Perkin–Elmer PHI 5000C ESCA system using Al-K_α radiation to determine the surface electronic states of the catalysts. Similarly, the Co–B sample was also dried in situ in pure Ar atmosphere to avoid oxidation. All the binding energy values were calibrated by using $C_{1s} = 284.6$ eV as a reference. The surface composition was determined by using 0.13 and 2.50 as the PHI sensitivity factors for B_{1s} and $Co_{2p_{3/2}}$, respectively, as offered by the Perkin–Elmer Company [22].

2.3. Activity test

Liquid phase hydrogenation of acetonitrile was carried out in a 200-ml stainless autoclave containing 1.0 g catalyst, 10 ml CH_3CN, and 30 ml EtOH at 1.0 MPa H_2 pressure, 373 K. In order to ascertain the role of mass transfer, the catalyst amount was varied from 0.5 g to 2.0 g and the speed of agitation was varied from 1000 to 1700 rpm. In view of the observation that the reaction rate was independent of the stirring rate and that it varied linearly with catalyst amount, it could be concluded that the stirring rate of 1000 rpm was high enough so that the hydrogenation rates were independent of mass transfer. The initial rate of reaction was obtained by measuring the drop of P_{H_2} within the first 0.5 h, from which both the specific activity (the H_2 uptake rate per gram of cobalt, $R_H{}^m = \text{mol}\,h^{-1}\,g^{-1}$ Co) and the areal activity (the H_2 uptake rate per m^2 of the active surface area, $R_H{}^S = \text{mol}\,h^{-1}\,g^{-1}$ Co) were calculated using the ideal gas equation. $R_H{}^S$ could be considered as the intrinsic activity since the effect of metal dispersion has been excluded. During the reaction, the H_2 was refilled to 1.0 MPa once it dropped to 0.80 MPa and the reaction mixture was sampled every 60 min to determine the conversion and the selectivities by using a gas chromatograph (GC 102)

equipped with a FID. The conditions for the analysis were as follows: 2-m column filled with GDX-102/407, injector temperature 373 K, oven temperature 418 K, detector temperature 473 K, and carrier gas N_2, 30 ml/min. The reproducibility of the results was checked by repeating the runs at least three times and was found to be within acceptable limits (±5%).

3. Results and discussion

3.1. Structural and electronic characteristics of the as-prepared catalysts

The SAED pictures of the fresh Co–B sample displayed many diffractional cycles indicative of the amorphous structure [23], which disappeared after treatment at high temperature. The XRD patterns, as shown in Fig. 1, also demonstrated that the fresh Co–B sample was present in a typical amorphous structure since only a broad peak around $2\theta = 45°$ was observed [24–27]. No appreciable change in the XRD pattern was observed when the Co–B sample was treated at a temperature below 473 K. However, when the treatment temperature further increased, the broad peak disappeared and a lot of sharp diffractional peaks corresponding to metallic Co, crystalline Co_2B, and Co_3B alloy species appeared gradually, showing the beginning of the crystallization process, during which partial decomposition of Co–B alloy also occurred. The degrees of both the crystallization and the decomposition of the Co–B amorphous alloy increased with increased treatment temperature and reached a maximum at 773 K, since no more changes in the XRD patterns were observed when the treatment temperature further increased. The amorphous structure was further confirmed by EXAFS on the $\chi(k)k^3$ Co edge, from which the RDF curves could be obtained by the fast Fourier transformation. As shown in Fig. 2, only one FT peak around $R = 2.0$ Å was found for the fresh Co–B sample, indicating that it had no long-range ordering structure but only a short-range ordering structure [28]. After the sample had been treated at 773 K for 2 h, the intensity of the original peak increased profoundly and two small additional peaks appeared at longer distances, showing the transformation from an amorphous structure to a well-ordered crystalline structure. The DSC analysis, as shown in Fig. 3, revealed that the crystallization of the Co–B amorphous alloy involved two steps corresponding to two exothermic peaks. The first small peak, around 480 K, was indicative of a rearrangement of the Co–B amorphous alloy structure [29], while the second large peak, corresponding to

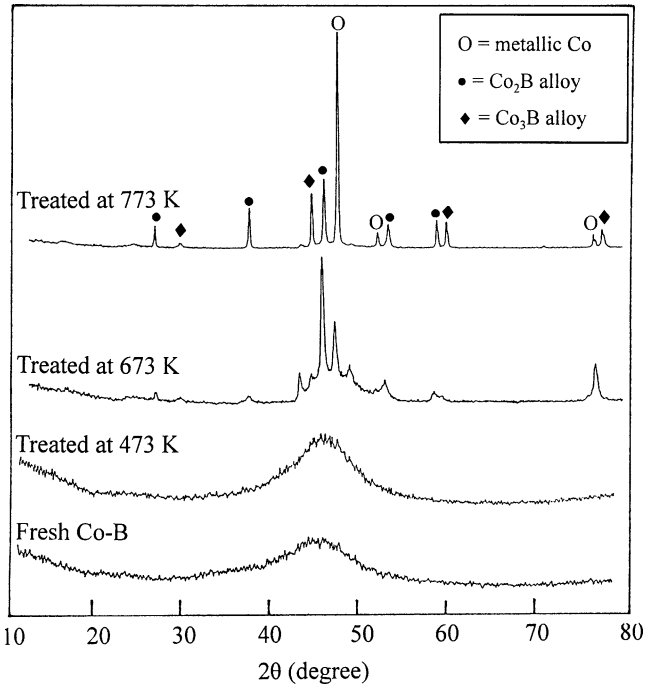

Fig. 1. XRD patterns of the Co–B sample treated at different temperatures.

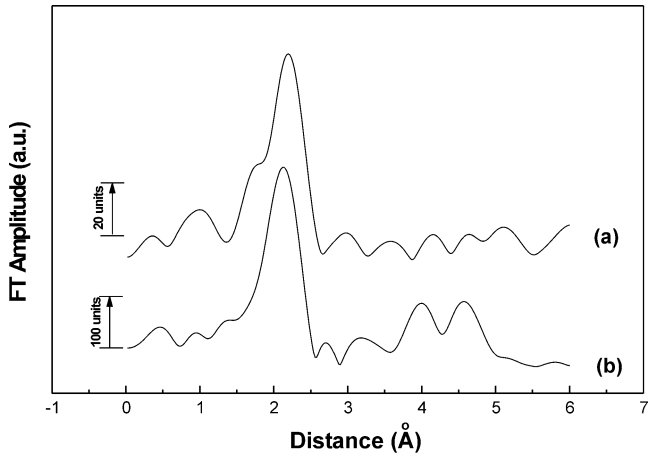

Fig. 2. RDF curves of (a) the fresh Co–B sample and (b) the Co–B sample after being treated at 773 K in H_2 flow for 2 h.

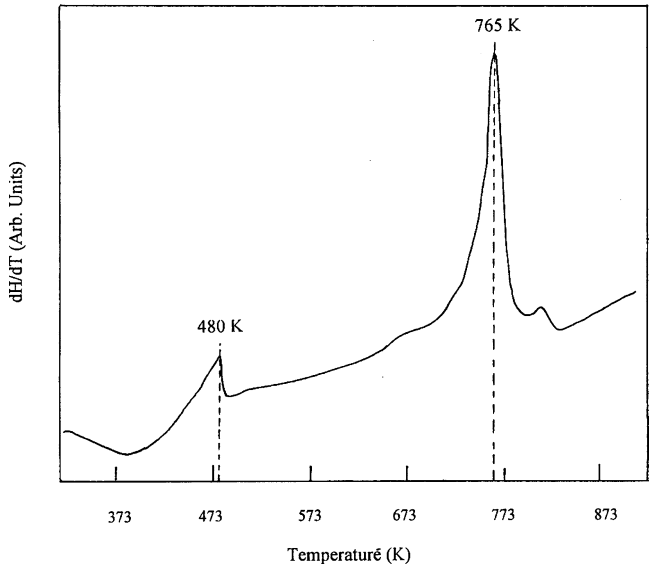

Fig. 3. DSC profile of the Co–B amorphous alloy catalyst.

Table 1
Structural properties of the as-prepared catalysts

Catalyst	Bulk composition	S_{act} (m^2/g)	Co-edge EXAFS data		
			R_{Co-Co} (Å)	Coordination number (N)	D–W factor σ (nm)
Fresh Co–B	$Co_{75.4}B_{24.6}$	15.8	2.42	8.7	0.0248
Cryst. Co–B	$Co_{75.4}B_{24.6}$	7.8	2.55	10.6	0.0212
Co powder	Co	3.5	2.50	9.7	0.0220
Raney Co	–	30.9	2.51	9.9	0.0226

765 K, corresponded to the occurrence of the crystallization of the Co–B amorphous alloy.

Table 1 lists the bulk compositions and the S_{act} values as well as some structural parameters calculated from the EXAFS data by using the EXAFS (II) program [30]. One can see that the crystallization has no appreciable influence on the composition of the Co–B sample, but it did cause an abrupt decrease in S_{act} owing to the gathering of small particles at high temperature, as could be seen from either SEM or TEM morphologies. The SEM micrographs, as shown in Fig. 4, demonstrated that the fresh Co–B sample displayed a homogeneous morphology composed of ultrafine Co–B alloy particles with average sizes between 50 and 100 nm. This homogeneous distribution was destroyed and big lumpsappeared gradually when the Co–B sample was treated at elevated temperatures from 573 to 773 K. Similar results were also obtained by TEM micrographs. Meanwhile, the Co–B amorphous alloy had a shorter Co–Co bonding length (R_{Co-Co}), a lower coordination number (N) for Co active sites, and a higher D–W factor (σ) than the crystallized Co–B, Co powder, and Raney Co catalysts, showing that the Co active sites in the Co–B amorphous catalyst (1) had a stronger synergistic effect between each other; (2) were more highly unsaturated; and (3) distributed more homogeneously [31].

The XPS spectra, as shown in Fig. 5, revealed that nearly all the cobalt species were present in the metallic state, corresponding to a binding energy (BE) of 778.3 eV at the $Co_{2p_{3/2}}$ level. Whereas, the boron species were present in both the elemental and oxidizing forms with BE values of 188.2 and 192.5 eV, respectively. Comparing the B_{1s} binding energy for elemental B with that of pure boron (187.2 eV), it is immediately found that the elemental B is positively charged. Chen et al. also observed the positive BE shift of the alloying B in the Co–B and Ni–B amorphous alloys [12]. They believed that partial electrons transferred from the alloying B to oxygen in the neighboring B_2O_3 rather than to the metallic Ni, since the negativity of B is higher than Ni. In contrast, the alloying B accepted partial electrons from the metallic Ni. They supplied excellent experimental results to support their conclusion, which showed that the CO adsorption produced higher heat on K^+/Ni than on the Ni, while the CO adsorption on the Ni–B amorphous alloy produced lower heat than on the Ni. These results have been confirmed by our experiments. As the K^+ donates electrons to Ni, it seems quite natural to conclude that the alloying B might attract electrons from the Ni. However, we think that the above conclusion about the electronic interaction might not be exactly true due to the different roles of K^+ and B in the K^+/Ni and Ni–B, respectively. As is well known, the K^+ donated electrons to the Ni in the K^+/Ni, but it did not change the structure of Ni active center. However, the role of B in Ni–B was

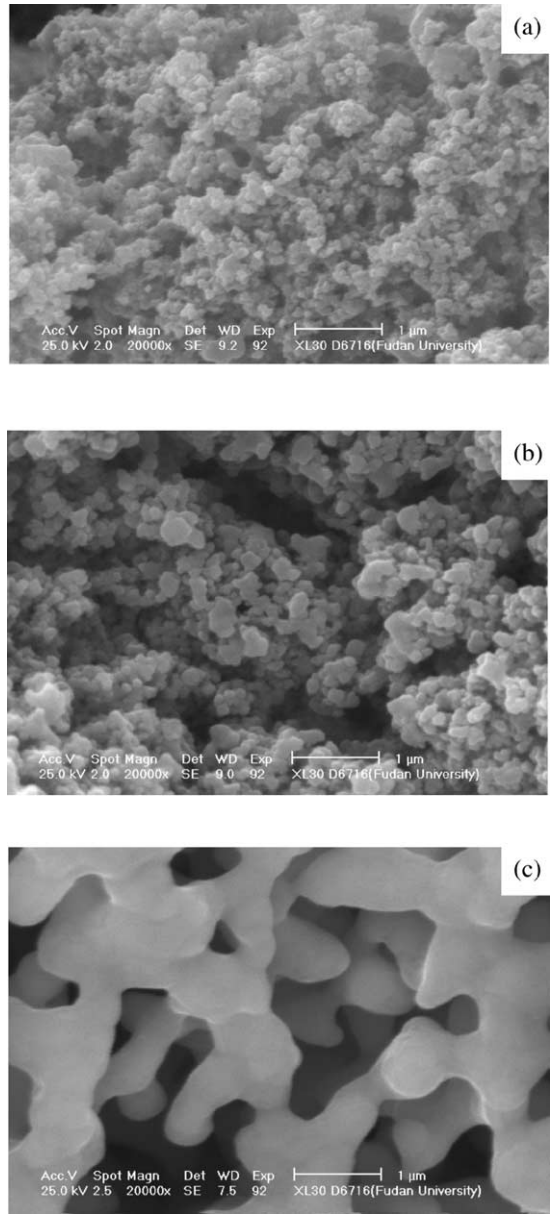

Fig. 4. SEM morphologies of (a) the fresh Co–B sample and the Co–B sample after treatment at (b) 573 K, (c) 773 K in H_2 flow for 2 h.

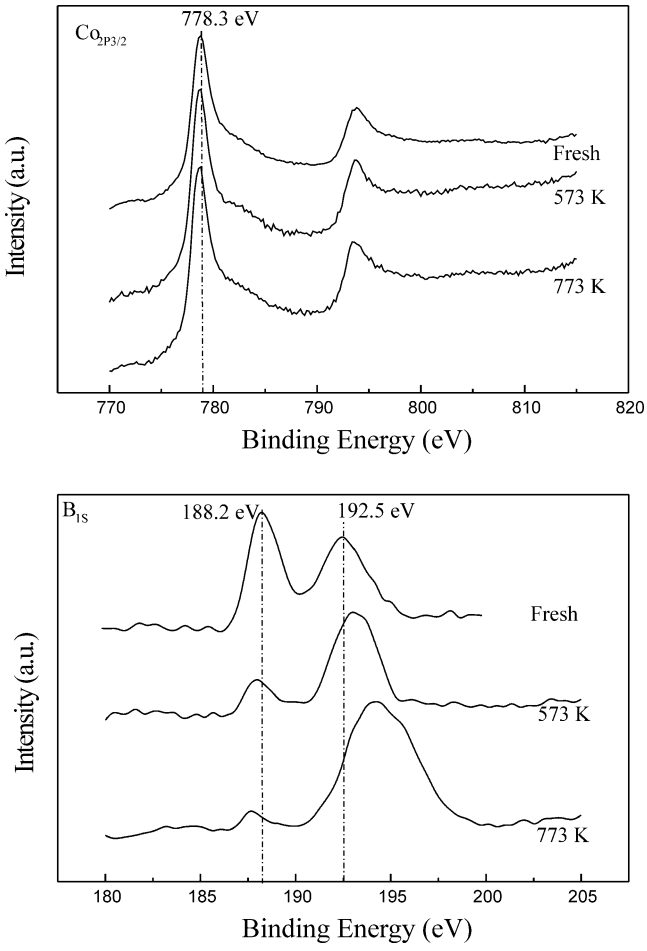

Fig. 5. XPS spectra of the Co–B amorphous alloy catalyst as received or the Co–B sample treated at different temperatures.

more complex. Besides the electronic interaction, modification of Ni with B may also change the structural characteristics of the Ni active sites. For example, the interaction between the elemental B and the metallic Ni resulted in Ni–B amorphous alloy while the pure Ni is present in the crystalline form. In addition, according to our EXAFS characterizations [31], the presence of the alloying B may result in the highly unsaturated coordination of the Ni active sites and the shorter bonding length between neighboring Ni atoms. The change of these structural properties might also change the CO adsorption heat on the Ni active center. Perhaps, the CO adsorption model on the Ni active center might also be changed. Thus, it might not be convincing to conclude the electron transfer between Ni and B in the Ni–B amorphous alloy by simply comparing the CO adsorption heat on the K^+/Ni and the Ni–B sample because the former might be attributed to merely the electronic interaction between K^+ and Ni while the latter might be attributed to both the electronic interaction between Ni and B and the structural modification of the Ni active center by the alloying B. Perhaps the XPS characterization could supply more direct evidence for the electron transfer in the Ni–B and the Co–B amorphous alloys. We concluded that the alloying B might donate partial electrons to the metallic Ni or Co based on the following considerations: (1) The XPS spectra of the Ni–B amorphous alloy revealed that the BE of the alloying B shifted positively by 1.0 eV in comparison with the pure B, indicating that the alloying B lost partial electrons. Such phenomena were also observed by Chen et al. [12]. However, they pointed out that the alloying B donated electrons to the neighboring boron oxide rather than to the metallic Ni. To confirm the direction of the electron transfer in the Ni–B amorphous alloy, a mixture of the elemental B and the B oxide was prepared by decomposing the KBH_4 in acidic solution in the presence of Cu^{2+}. The XRD patterns demonstrated that all the Cu species were present in a pure metallic state (crystalline Cu); i.e., no Cu–B alloy was formed. In that case, the XPS spectra of the elemental B does not display significant BE shift, implying that the positive shift in the BE value of the elemental B occurred only in the presence of metallic Ni or Co, rather than in the presence of the neighboring B_2O_3. (2) Yoshida et al. supplied more convincing evidence to support our conclusion [32] by the XPS characterizations of the Ni–B amorphous alloy obtained by the rapid quenching technique. Unlike the Ni–B amorphous alloy obtained by chemical reduction with KBH_4, which contained comparable oxidized B species due to the decomposition of KBH_4 in aqueous solution, the Ni–B amorphous alloy obtained by the rapid quenching technique contained very little or even no oxidized B species, since the preparation was performed exactly in the absence of O_2. Trace oxidized B species on the surface of the Ni–B alloy might be detected due to surface oxidation during the treatment. The XPS spectra revealed that, after the treatment with dilute HNO_3, neither the oxidized B species nor the oxidized Ni species were present in the as-prepared Ni–B amorphous alloy. In that case, the XPS spectra also displayed a positive BE shift of the alloying B, which was obviously due to its electron donation to the metallic Ni in the Ni–B alloy, since no other species were present at all. (3) The theoretical calculations using ab initio DFT method also demonstrated that the alloying B donated partial electrons to Ni in the Ni–B amorphous alloy, as shown in Table 2. (4) Our recent experimental re-

Table 2
The electron populations of Ni and B atoms in Ni_MB_2 ($M = 1$–4) clusters[a]

Ni–B model	B [1]	B [2]	Ni [1]	Ni [2]	Ni [3]	Ni [4]
Ni_2B_2	+0.2812	+0.2812	−0.2812	−0.2812		
Ni_3B_2	+0.2301	+0.2301	−0.1652	−0.1475	−0.1475	
Ni_4B_2	+0.2962	+0.2962	−0.1481	−0.1481	−0.1481	−0.1481

[a] The symbols "+" and "−" represent electron-deficient and electron-enriched, respectively.

sults revealed that the metallic Ni in the Ni–B amorphous alloy possessed much stronger antioxidation ability than the pure Ni, showing that the presence of the alloying B in the Ni–B amorphous alloy could effectively protect the metallic Ni from oxidation. This might be more evidence to support our conclusion since the stronger oxidation resistance of the metallic Ni in the Ni–B amorphous alloy might be attributed to the electron donation of the alloying B which made the metallic Ni electron-enriched [33]. Thus, similarly to Nitta's group [34–37], Lee's group [38,39], and Yoshida's group [32], we concluded that partial electrons transferred from the elemental B to the metallic Ni or Co in the Ni–B or Co–B amorphous alloy, respectively, making the metallic Ni or Co electron-enriched while the elemental B is electron-deficient. The above conclusion could be explained by the assumption of Imanaka et al. that the bonding electrons of the B occupied the vacant *d*-orbitals of metallic Ni or Co [35]. The failure to observe the BE shift of the metallic Ni or Co could be understood by considering its relatively greater atomic weight compared to that of the B atom [40]. During the heating treatment, the content of alloying B decreased while the amount of oxidizing B increased gradually with the increase temperature, indicating the surface oxidation of the boron species at high temperature owing to the presence of trace oxygen in N_2 flow. However, both the position and the strength of the XPS peaks of the $Co2p_{3/2}$ level remained unchanged, this was mainly attributed to the alloying B which protected the surface Co from oxidation [41]. Besides the BE shift of the elemental B, the BE value of the oxidizing B also shifted positively from 192.5 to 194.1 eV during the heating treatment, possibly due to the transformation from BO_2^- to B_2O_3 [42]. Comparing the bulk composition of the Co–B amorphous alloy determined by the ICP analysis ($Co_{75.4}B_{24.6}$) with that of the surface composition determined by XPS spectra ($Co_{53.9}B_{46.1}$), it was obvious that the Co–B amorphous alloy was surface-enriched with the boron species.

3.2. Reaction route of acetonitrile hydrogenation

The composition of the reaction mixture as a function of time during the liquid phase CH_3CN hydrogenation over the Co–B amorphous alloy catalyst is plotted in Fig. 6a. According to the change of CH_3CN conversion, one can see that the hydrogenation rate decreased gradually with the reaction time. This could be attributed to the strong adsorption of $C_2H_5NH_2$ and/or $(C_2H_5)_2NH$ on the surface of metallic Co owing to the lone pair electrons on the N atom, which may inhibit the adsorption of reactants, and in turn, may retard the hydrogenation [43]. Important evidence supporting the above conclusion was that the reaction rate could be considerably enhanced by adding small amounts of H_2O, which may connect, with the N atom in $C_2H_5NH_2$ and $(C_2H_5)_2NH$ molecules via a hydrogen bonding and in turn, inhibited their adsorption on the Co active sites. Concerning the selectivities, both the $C_2H_5NH_2$ (primary amine) and

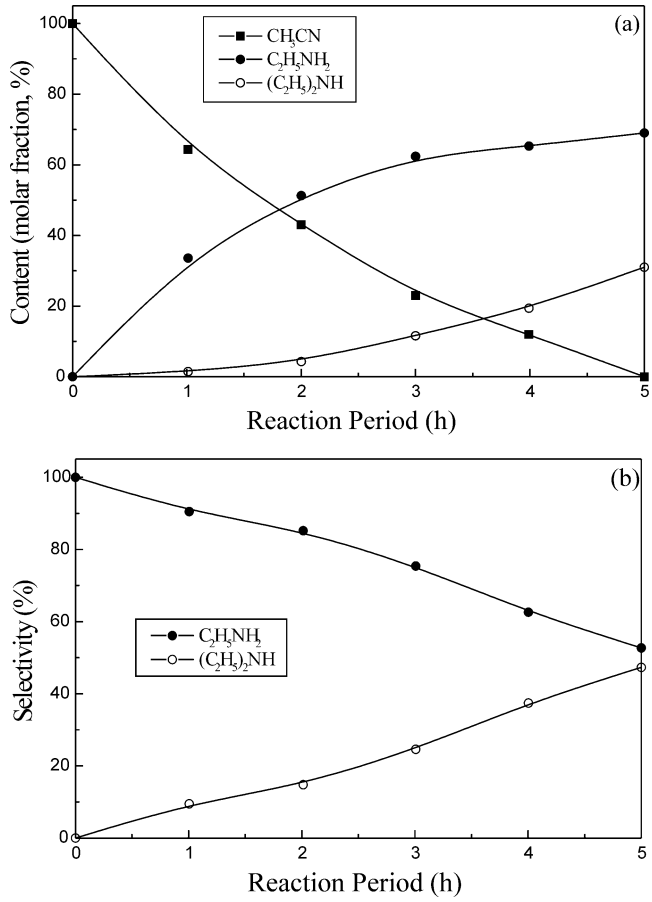

Fig. 6. Dependence of (a) the composition of the reaction product and (b) the selectivities to ethylamine and diethylamine on the reaction time during the liquid phase acetonitrile hydrogenation catalyzed by the Co–B amorphous alloy. Reaction conditions: 1.0 g catalyst, 10 ml CH_3CN, 40 ml EtOH, $T = 373$ K, $P_{H_2} = 1.0$ MPa, stirring rate = 1000 rpm.

the $(C_2H_5)_2NH$ (secondary amine) were identified while no significant $(C_2H_5)_3N$ (tertiary amine) was observed throughout the reaction process. Although the yields of both $C_2H_5NH_2$ and $(C_2H_5)_2NH$ increased gradually, owing to increased CH_3CN conversion, selectivities to these two products changed in opposite ways. The selectivity to $C_2H_5NH_2$ decreased while the selectivity to $(C_2H_5)_2NH$ increased with the reaction time, as shown in Fig. 6b. These results furnished evidence for the Braun mechanism for the nitrile hydrogenation [6,44,45]. As shown in the following scheme, a reactive intermediate, aldimine($CH_3CH{=}NH$), was formed, which could result in either the primary amine via its further hydrogenation or the secondary amine via its condensation reaction with the primary amine,

$$CH_3C{\equiv}N \overset{+H_2}{\rightarrow} CH_3CH{=}NH \overset{+H_2}{\rightarrow} CH_3CH_2NH_2, \qquad \text{(R1)}$$

$$CH_3CH{=}NH + CH_3CH_2NH_2 \overset{-NH_3}{\rightarrow} CH_3CH{=}NCH_2CH_3 \overset{+H_2}{\rightarrow} CH_3CH_2NHCH_2CH_3. \qquad \text{(R2)}$$

The relative contents of primary and secondary amines in the reaction mixture were mainly dependent on the competition

between hydrogenation (R1) and condensation (R2) [46]. High selectivity to $C_2H_5NH_2$ was obtained at low CH_3CN conversion since the condensation could not take place or proceeded very slowly due to the extremely low $C_2H_5NH_2$ concentration. With the increase of CH_3CN conversion, more and more $C_2H_5NH_2$ was accumulated, which enhanced the condensation rate and, in turn, favored the formation of $(C_2H_5)_2NH$, resulting in a decrease of the selectivity to $C_2H_5NH_2$.

3.3. Kinetic studies of acetonitrile hydrogenation

Fig. 7 shows the dependence of the initial reaction rate (R_H^m) on the concentration of CH_3CN and the pressure of hydrogen, which revealed that the hydrogenation reaction was zero-order with respect to CH_3CN while first-order with respect to hydrogen. A possible explanation was that both CH_3CN and H_2 were adsorbed competitively by the same Co active sites. The adsorption of CH_3CN was so strong that it reached a saturated concentration on the surface of the catalyst even at a very low concentration in the liquid phase and thus, the change of the CH_3CN concentration had no significant influence on the hydrogenation rate. However, the adsorption of hydrogen was relatively weak and its surface concentration never reached saturation under the present conditions. Thus, the surface concentration of hydrogen increased with increased P_{H_2} according to the Langmuir isothermal equation [47], which could account for the promoting effect of P_{H_2} on the hydrogenation rate. Besides the effect on the hydrogenation activities, it was also found that the selectivity to $C_2H_5NH_2$ increased slightly with an increase of either the hydrogen pressure or the CH_3CN concentration, as shown in Fig. 8. The promoting effect of P_{H_2} on the selectivity to $CH_3CH_2NH_2$ could be understood by considering the reaction mechanism [46]. Although both (R1) and (R2) involved hydrogenation, the key factor determining the selectivity to $CH_3CH_2NH_2$ or to $CH_3CH_2NHCH_2CH_3$ was the competition between the hydrogenation of the $CH_3CH{=}NH$(aldimine) and the condensation of the $CH_3CH{=}NH$ with the $CH_3CH_2NH_2$. From the above mechanism, increased H_2 pressure may favor the hydrogenation of $CH_3CH{=}NH$, leading to the desired product $CH_3CH_2NH_2$. However, there was no direct relationship between H_2 pressure and the condensation reaction. On the contrary, the increase of H_2 pressure may increase the con-

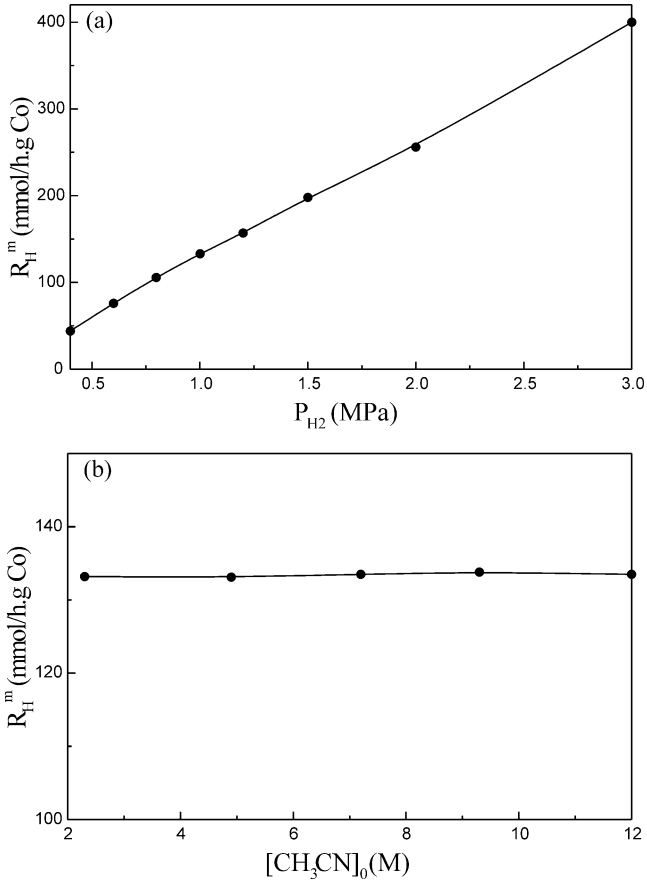

Fig. 7. Effects of (a) the pressure of hydrogen and (b) the concentration of acetonitrile on the initial rate of acetonitrile hydrogenation over the Co–B amorphous catalyst. Other reaction conditions are given in Fig. 6.

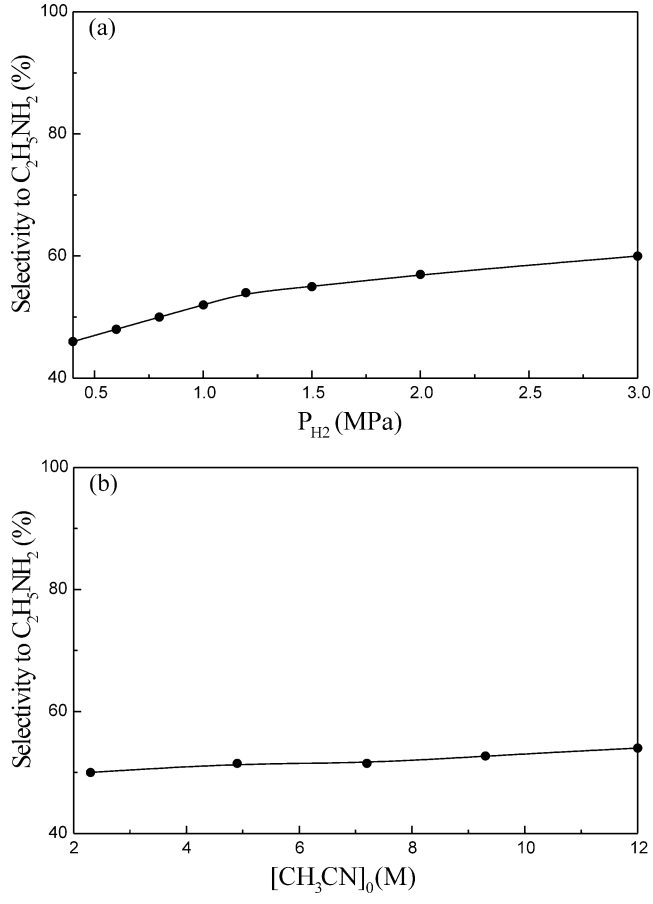

Fig. 8. Dependence of the selectivity to ethylamine on (a) the hydrogen pressure and (b) the acetonitrile concentration in the liquid phase acetonitrile hydrogenation over the Co–B amorphous catalyst. Other reaction conditions are given in Fig. 6.

sumption of $CH_3CH{=}NH$ and in turn decrease the condensation rate. Thus, the increase of H_2 pressure may increase the selectivity to $CH_3CH_2NH_2$. The positive influence of the CH_3CN concentration on the selectivity to $C_2H_5NH_2$ could be interpreted in terms of the accumulation of more ammonia resulting from the formation of the secondary amine. It was widely accepted that an increase in the ammonia concentration could effectively inhibit the formation of secondary amines and in turn could promote the selectivity to primary amines [48]. The promoting effect of ammonia on the selectivity to the primary amines could be explained by the following scheme proposed by Schwoeleger and Adkins [49,50]:

$$CH_3CH{=}NH + NH_3 \rightleftharpoons CH_3CH\begin{matrix}\diagup NH_2\\ \diagdown NH_2\end{matrix} \xrightarrow{+H_2} CH_3CH_2NH_2 + NH_3.$$

The rate of CH_3CN hydrogenation increased rapidly with the increase of the reaction temperature, as found in the hydrogenation of most other nitriles. According to the linear relationship between $R_H{}^m$ and $1/T$, the apparent activation energy was determined as 46 kJ/mol over the Co–B amorphous catalyst. In contrast to the effect on the activities, a slight decrease of about 10% in the selectivity to $C_2H_5NH_2$ was observed when the reaction temperature increased from 323 to 423 K. Such a negative effect could be understood by considering the higher activation energy of the condensation reaction (usually > 100 kJ/mol) leading to the secondary amine [51,52].

3.4. Performance of various catalysts

Table 3 summarizes the catalytic properties of various catalysts in liquid phase hydrogenation of CH_3CN, including the initial reaction rate, the reaction time corresponding to total conversion of CH_3CN, and the selectivities to primary, secondary, and tertiary amines obtained in the reaction mixture after the total conversion of CH_3CN. The selectivity over the Co powder catalyst was not available here since the reaction rate was too slow to reach the complete CH_3CN conversion. From Table 3, the following conclusions were drawn.

1. The Ni-based catalysts exhibited much higher activity than the Co-based catalysts, owing to the relatively stronger adsorption of the reactants (both hydrogen and acetonitrile, as well as aldimine intermediate) [53]. However, in the absence of ammonia, the selectivity to $C_2H_5NH_2$ on either the Ni–B amorphous catalyst or the Raney Ni was very low. In contrast to the Co-based catalysts over which only the secondary amine was identified as the side product, a comparable amount of tertiary amine was detected besides the secondary amine over the Ni-based catalysts. Increasing the B content in the Ni–B alloy may slightly increase the selectivity to the primary amine due to the decrease in the selectivities to both the secondary and tertiary amines. However, even over the $Ni_{66.7}B_{33.3}$, which contained the maximum B content in the Ni–B amorphous alloys prepared under the present conditions, the selectivity to the primary amine was still much lower than that over the $Co_{75.4}B_{24.6}$, showing that the Ni–B amorphous alloy catalysts were not suitable for the title reaction. The higher content of the secondary and tertiary amines in the hydrogenation product on Ni-based catalysts, corresponding to the lower selectivity to the primary amine, could be attributed to the relatively stronger adsorption of the product, $C_2H_5NH_2$, on Ni-active sites than on Co-active sites, which may enhance the condensation rate, leading to the secondary amine and even the tertiary amine [53].

2. Concerning the activities of different Co-based catalysts, one can see that the specific activities ($R_H{}^m$) decreased in the order Raney Co > Co–B amorphous catalyst $\gg$ crystallized Co–B catalyst $\gg$ Co powder catalyst. This was not in accordance with the change of the areal activities ($R_H{}^S$), which decreased in the order Co–B amorphous catalyst > Raney Co > crystallized Co–B catalyst > ultrafine Co. Thus, the higher $R_H{}^m$ of Raney Co than of the Co–B amorphous catalyst was mainly attributed to its much higher ac-

Table 3
Hydrogenation of acetonitrile(CH_3CN) on various catalysts[a]

Catalyst	$R_H{}^m$ (mmol h^{-1} g^{-1} M)	$R_H{}^S$ (mmol h^{-1} m^{-2} M)	Reaction time[b] (min)	Selectivity (%)		
				$C_2H_5NH_2$	$(C_2H_5)_2NH$	$(C_2H_5)_3N$
Fresh $Co_{75.4}B_{24.6}$	133.8	8.47	297	53.0	47.0	~0
Fresh $Ni_{80.7}B_{19.3}$	151.5	10.0	238	24.0	45.0	31.0
Fresh $Ni_{75.2}B_{24.8}$	169.5	12.1	201	28.0	44.8	27.2
Fresh $Ni_{66.7}B_{33.3}$	196.7	15.2	185	37.0	46.8	16.2
Raney Ni	432.8	10.0	116	21.4	37.4	41.2
Cryst. $Co_{75.4}B_{24.6}$[c]	42.6	5.46	678	44.6	55.4	~0
Raney Co	205.4	6.65	152	38.8	61.2	~0
Co powder[d]	11.1	3.10	–	–	–	–

[a] Reaction conditions: 1.0 g catalyst, 10 ml CH_3CN, 40 ml EtOH, $T = 373$ K, $P_{H_2} = 1.0$ MPa, stirring rate = 1000 rpm, M = Co or Ni.

[b] The time corresponding to the total conversion of CH_3CN.

[c] The crystallized Co–B catalyst obtained by treating the Co–B amorphous alloy at 773 K for 2 h in H_2 flow.

[d] The reaction is too slow to detect the time for total CH_3CN conversion and the selectivities.

tive surface area (S_{act}), as shown in Table 1. Besides the decrease of the S_{act} during the heating treatment (see Table 1), the higher $R_H{}^m$ of the Co–B amorphous catalyst than of the corresponding crystallized Co–B catalyst could be mainly attributed to the remarkable decrease in the intrinsic activity during the crystallization (see the $R_H{}^S$ values in Table 1), which could be understood by considering both the structural effect and the electronic effect. The structural effect mainly referred to the unique amorphous structure. According to the structural parameters calculated from the EXAFS data, as shown in Table 1, the Co–B amorphous catalyst had shorter Co–Co bonding length (R_{Co-Co}), lower coordination number (N) of Co active sites, and higher D–W factor (σ) than the corresponding crystallized Co–B catalyst, implying a stronger synergistic effect between Co active sites, more highly unsaturated Co active sites, and a more homogeneous distribution of the Co active sites. These factors have been claimed to be favorable for the dissociative adsorption of hydrogen molecules and, in turn, to enhance hydrogenation activity [54,55]. Regarding the electronic effect, the above XPS spectra reveale that in the Co–B amorphous alloy, Co is electron-enriched while B is electron-deficient owing to their electronic interaction. After crystallization, electronic interaction decreased or even disappeared due to the decomposition of the Co–B alloy, as confirmed by the aforementioned XRD patterns. On one hand, the relative high density of electrons on the Co active sites may repel the lone pair electrons on the N atom in the CN group and in turn, may weaken the adsorption strength between CH_3CN molecules and Co active sites. This was favorable for the adsorption of H_2 taking into account that the adsorption of CH_3CN and H_2 molecules was competitive on the same Co active sites. Thus, more H_2 could be adsorbed by the Co active sites, which enhanced the hydrogenation activity, since the reaction was first-order with respect to hydrogen, while independent of the CH_3CN concentration. On the other hand, according to the adsorption model of the nitrile [56], the electronic interaction between the C≡N group and the Co active sites was the forward donation of the electrons from the highest occupied molecular orbital (HOMO) of the C≡N bonding, i.e., from the $\pi_{C\equiv N}$ to the d_{z^2} and S orbitals of the Co atom, and the back donation from the $d_{x^2-y^2}$ orbital of the Co atom to the lowest unoccupied molecular orbital (LUMO), i.e., $\pi^*_{C\equiv N}$. Increased back donation may favor the C≡N bond dissociation since the $\pi^*_{C\equiv N}$ was an antibonding orbital [57]. Thus, from a hydrogenation point of view, an increase in the electron density on the Co active sites due to the charge transfer from alloying B should lead to increased back donation, thereby weakening the C≡N bond and in turn facilitated its hydrogenation. Furthermore, the in situ XPS characterization demonstrates that the presence of the alloying B in the Co–B amorphous alloy could effectively protect metallic Co from oxidation. This could also account for the higher activity of the Co–B amorphous alloy than that of the crystallized Co–B alloy since only the metallic Co served as the active sites for hydrogenation of CH_3CN and other intermediates while the oxidized Co was inactive.

3. As shown in Table 3, the selectivity to $C_2H_5NH_2$ decreased in the order Co–B amorphous catalyst > crystallized Co–B catalyst > Raney Co. According to the reaction mechanism, the selectivities to the primary and secondary amines were mainly dependent on the competition between the hydrogenation of the $CH_3CH{=}NH$ leading to the primary amine and the condensation between $CH_3CH{=}NH$ and $C_2H_5NH_2$ leading to the secondary amine [6]. Such condensation may proceed through a nucleophilic attack of the N atom in the $C_2H_5NH_2$ molecule on the C atom connecting with the N atom in the $CH_3CH{=}NH$ molecule, as shown in the following diagram [58].

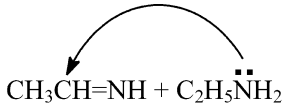

Thus, the more positive charges on the C atom and the more negative charges on the N atom may facilitate the condensation reaction. Taking into account that the metallic Co in the Co–B amorphous alloy was electron-enriched, the excellent selectivity to $C_2H_5NH_2$ on the Co–B amorphous catalyst could be explained based on the above assumption. On one hand, the electron enrichment of the Co active sites could effectively repel the lone pair electrons on the N atom in the $C_2H_5NH_2$ molecule and thus might weaken its adsorption on the Co surface. This could effectively inhibit the condensation between the $C_2H_5NH_2$ and the $CH_3CH{=}NH$, since the adsorption of both $C_2H_5NH_2$ and the $CH_3CH{=}NH$ was necessary for such condensation. On the other hand, as discussed above, the high electron density on the Co active sites could increase the back donation of electrons to the $\pi^*_{C\equiv N}$, making the C atom connecting with the N atom in the $CH_3CH{=}NH$ molecule less positive, which could also retard the condensation reaction. Furthermore, the increased back donation of electrons to the $\pi^*_{C\equiv N}$ could also weaken the C=N bond, making the C=N bond activated and, in turn, making its hydrogenation more facilitated. As a summary, owing to the electronic interaction between Co and alloying B, the Co–B amorphous alloy was favorable for the hydrogenation reaction while unfavorable for the condensation reaction, resulting in the higher selectivity to the primary amine, i.e., $C_2H_5NH_2$. The crystallized Co–B catalyst displayed lower selectivity to $C_2H_5NH_2$ due to the decrease in the electronic interaction, since partial decomposition of the Co–B alloy occurred during the crystallization process. Raney Co showed even lower selectivity to $C_2H_5NH_2$ than the crystallized Co–B catalyst, since no such electronic interaction was present at all. Besides the electronic interaction, the alloying B in the Co–B amorphous alloy could protect metallic Co from oxidation, which was also favorable for keeping the high selectivity to $C_2H_5NH_2$ since, according to the aforementioned reaction mechanism (R1) and (R2), the rapid hydrogenation of $CH_3CH{=}NH$ may result in high selectivity to $C_2H_5NH_2$.

4. Conclusion

The above results demonstrated that the amorphous Co–B was powerful for the liquid phase hydrogenation of acetonitrile to ethylamine, owing to its higher activity and better selectivity to the desired product. The factors accounting for the promoting effect on the activity were, on one hand, the shorter Co–Co bonding length ($R_{Co–Co}$), lower coordination number (N) of Co active sites, and higher D–W factor (σ), which accelerated the hydrogenation, since they were favorable for the adsorption of the H_2; on the other hand, the electronic interaction between Co and alloy B, which facilitated the hydrogenation of the C≡N bond, since higher electron density on the Co active sites could activate the C≡N bond by back donation of electrons to the $\pi^*_{C\equiv N}$, an antibonding orbital. The higher selectivity to primary amine on the Co–B amorphous catalyst was mainly attributed to the electronic interaction between Co and alloy B, making Co active sites electron-enriched, which could enhance the hydrogenation of $CH_3CH{=}NH$ leading to primary amine since more electrons on the Co active sites may activate the C=N bond. Such electron-enriched Co active sites could also retard the condensation reaction between $CH_3CH{=}NH$ and $C_2H_5NH_2$ molecules, leading to the secondary amine, since the adsorption of $C_2H_5NH_2$ on the Co active sites decreased due to the repelling for the lone pair electrons on the N atom and the C atom connecting with the N atom in the $CH_3CH{=}NH$ became less positive due to the increased back donation of electrons from Co atoms. The catalytic activity and selectivity of the Co–B amorphous catalyst could be further improved by adjusting the B content in the Co–B amorphous alloy or adding other additives, including the bimetallic catalysts and supported catalysts. These works are under way.

Acknowledgments

This work was supported by the National Natural Science Foundation of China (29973025), the Natural Science Foundation of Shanghai Science and Technology Committee, and the Shanghai Education Committee (01DZ01).

References

[1] H. Greenfield, Ind. Eng. Chem. Prod. Res. Develop. 6 (1967) 142.
[2] J. Pasek, N. Kostova, B. Dvorak, Collect. Czech. Chem. Commun. 46 (1981) 1011.
[3] C. de Bellefon, P. Fouilloux, Catal. Rev. Sci. Eng. 36 (1994) 459.
[4] K. Weissermel, H.-J. Arpe, Industrial Organic Chemistry, 2nd ed., VCH, Weinheim, 1993.
[5] D. Gavroy, C. Joly-Vuillemin, G. Cordier, P. Fouilloux, H. Delmas, Catal. Today 24 (1995) 103.
[6] J. Volf, P. Josef, Stud. Surf. Sci. Catal. 27 (1986) 105.
[7] M.J.F.M. Verhaak, A.J. van Dillen, J.W. Geus, Catal. Lett. 26 (1994) 37.
[8] G.W. Handdix, A.T. Bell, J.F. Reimer, J. Phys. Chem. 93 (1989) 5859.
[9] B. Coq, D. Tichit, S. Ribet, J. Catal. 189 (2000) 117.
[10] M.J.F.M. Verhaak, A.J. van Dillen, J.W. Geus, J. Catal. 143 (1993) 187.
[11] F.M. Cabello, D. Tichit, B. Coq, A. Vaccari, N.T. Dung, J. Catal. 167 (1997) 142.
[12] Y. Chen, Catal. Today 44 (1998) 3.
[13] J.F. Deng, H.X. Li, W.J. Wang, Catal. Today 51 (1999) 113.
[14] J.V. Jefimov, M.V. Glasov, L.I. Vornova, Chem. Technol. 38 (1986) 70.
[15] A. Molnar, G.V. Smith, M. Bartok, Adv. Catal. 36 (1989) 329.
[16] H.X. Li, Y.P. Xu, H. Li, J.F. Deng, Appl. Catal. A General 216 (2001) 51.
[17] H.X. Li, M.H. Wang, Y.P. Xu, Chem. Lett. (2000) 1048.
[18] H.X. Li, Y.P. Xu, J.F. Deng, New J. Chem. 23 (1999) 1059.
[19] H.X. Li, H. Li, M.H. Wang, Appl. Catal. A General 207 (2001) 129.
[20] H.X. Li, X.F. Chen, M.H. Wang, Y.P. Xu, Appl. Catal. A General 225 (2002) 117.
[21] H.X. Li, W. Wang, H. Li, J.F. Deng, J. Catal. 194 (2000) 211.
[22] Physical Electronic Division, Perkin–Elmer, Operator's Reference Manual for PHI PC Windows Software Version 1.2b, p. 274.
[23] S. Klein, J.A. Martens, R. Parton, K. Vercruysse, P.A. Jacobs, W.F. Maier, Catal. Lett. 38 (1996) 209.
[24] A. Yokoyama, H. Komiyama, H. Inoue, T. Masumoto, H.M. Kimura, J. Catal. 68 (1981) 355.
[25] H.X. Li, H.Y. Chen, S.Z. Dong, J.S. Yang, J.F. Deng, Appl. Surf. Sci. 125 (1998) 115.
[26] H. Yamashita, M. Yoshikawa, T. Funabiki, S. Yoshida, J. Chem. Soc. Faraday Trans. I 82 (1986) 1771.
[27] J. van Wonterghem, S. Mørup, C.J.W. Koch, S.W. Charles, S. Wells, Nature 322 (1986) 622.
[28] J.A. Schwarz, C. Contescu, A. Contescu, Chem. Rev. 95 (1995) 477.
[29] H. Yamashita, T. Funabiki, S. Yoshida, J. Chem. Soc. Chem. Commun. (1984) 868.
[30] J. Chen, G. Lu, L. Ma, Fudan Univ. Acta 28 (1989) 78.
[31] B. Shen, S. Wei, K. Fan, J.F. Deng, Appl. Phys. A 65 (1997) 295.
[32] S. Yoshida, H. Yamashita, T. Funabiki, T. Yonezawa, J. Chem. Soc. Faraday Trans. 1 80 (1984) 1435.
[33] W.L. Dai, H.X. Li, Y. Cao, M.H. Qiao, K.N. Fan, J.F. Deng, Langmuir, in press (2002).
[34] Y. Okamoto, Y. Nitta, T. Imanaka, S. Teranishi, J. Chem. Soc. Faraday Trans. 1 75 (1979) 2027.
[35] T. Imanaka, Y. Nitta, S. Teranishi, Bull. Chem. Soc. Jpn. 46 (1973) 1134.
[36] Y. Okamoto, Y. Nitta, T. Imanaka, S. Teranishi, J. Chem. Soc. Faraday Trans. 1 76 (1980) 998.
[37] Y. Okamoto, Y. Nitta, T. Imanaka, S. Teranishi, J. Catal. 64 (1980) 397.
[38] S.P. Lee, Y.W. Chen, J. Mol. Catal. A Chem. 152 (2000) 213.
[39] S.P. Lee, Y.W. Chen, Ind. Eng. Chem. Res. 40 (2001) 1495.
[40] H. Li, H.X. Li, W. Dai, Z. Fang, J.F. Deng, Appl. Surf. Sci. 152 (1999) 25.
[41] H.X. Li, W. Wang, H. Chen, J.F. Deng, J. Non-Cryst. Solids 281 (2001) 31.
[42] Y. Okamoto, Y. Nitta, T. Imanaka, S. Teranishi, J. Catal. 64 (1980) 397.
[43] J. Volf, J. Pasek, M. Duraj, Collect. Czech. Chem. Commun. 38 (1973) 1038.
[44] P.N. Chatterjee, R.A. Shaikh, A. Raj, A.P. Singh, Catal. Lett. 31 (1995) 301.
[45] P.N. Rylander, L. Hasbrouck, I. Karpenko, Ann. NY Acad. Sci. 214 (1973) 100.
[46] M. Morak, F. Krsnak, Czech Patent 152102, 1990.
[47] W.H. Weinberg, R.P. Merrill, Surf. Sci. 33 (1972) 493.
[48] D. Nowak, W. Jerzykiewicz, Przem. Chem. 49 (1972) 664.
[49] E.J. Schwoegler, H. Adkins, J. Am. Chem. Soc. 61 (1939) 3499.
[50] Y. Huang, W.M.H. Sachtler, Appl. Catal. A General 182 (1999) 365.

[51] Sh.A. Zelenaya, A.S. Basov, A.A. Pavlov, N.K. Petryakova, N.V. Gushin, Khim. Prom. Moscow 46 (1970) 11.
[52] M.I. Yakushin, P.V. Bazyleva, Khim. Prom. Moscow 44 (1968) 265.
[53] M. Kalina, J. Pasek, Kinet. Catal. 10 (1969) 574.
[54] A. Baiker, Faraday Discuss. Chem. Soc. 87 (1989) 239.
[55] H.X. Li, W.J. Wang, J.F. Deng, J. Catal. 191 (2000) 257.
[56] G.D. Yadav, M.R. Kharkara, Appl. Catal. A General 126 (1995) 115.
[57] A.R. Albert, J.T. Yates Jr., The Surface Scientists Guide to Organometallic Chemistry, Am. Chem. Society, Washington, DC, 1987, p. 29.
[58] P.N. Rylander, L. Hasbrouck, Eng. Ind. Tech. Bull. 11 (1979) 19.